Arabian Journal of Chemistry (2020) **13**, 474–480

King Saud University

Arabian Journal of Chemistry

www.ksu.edu.sa
www.sciencedirect.com

ORIGINAL ARTICLE

Luminescence properties of yttrium gadolinium orthovanadate nanophosphors and efficient energy transfer from VO_4^{3-} to Sm^{3+} *via* Gd^{3+} ions

Vishnu V. Jaiswal, Swati Bishnoi, G. Swati, Paramjeet Singh, Naina Lohia, Sivaiah Bathula, D. Haranath *

CSIR-National Physical Laboratory, Dr. K.S. Krishnan Road, New Delhi 110 012, India

Received 2 January 2017; accepted 22 May 2017
Available online 26 May 2017

KEYWORDS

Nanophosphor;
Energy transfer;
Photoluminescence;
Orthovanadate

Abstract In this paper, luminescence properties of orthovanadates, $Y_{1-x-y}Gd_xVO_4:ySm^{3+}$ (where $x = 0.05–0.50$, $y = 0.01–0.05$), and the energy transfer mechanism from VO_4^{3-} to Sm^{3+} via Gd^{3+} ions were investigated in detail. X-ray diffraction (XRD) analysis confirmed the crystalline phase for synthesized nanophosphor in a tetragonal structure with *I41/amd* space group. The average crystallite size estimated from XRD was ~28 nm. Field-emission scanning electron microscopy coupled with energy dispersive X-ray analysis revealed oval shaped morphology and composition of the nanophosphor, respectively. From high-resolution transmission electron microscopy observations, the particle sizes were found to be in the range 10–80 nm. The photoluminescence studies of $Y_{0.77}Gd_{0.20}VO_4:0.03Sm^{3+}$ nanophosphor under 311 nm excitation exhibits dominant emission peak at 598 nm corresponding to $^4G_{5/2} \rightarrow {}^6H_{7/2}$ transition. The energy transfer occurs from VO_4^{3-} to Sm^{3+} via Gd^{3+} ions was confirmed by applying Dexter and Reisfeld's theory and Inokuti-Hirayama model. Moreover, the energy transfer efficiencies and probabilities were calculated from the decay curves. Furthermore, Commission Internationale de l'Eclairage (CIE) color coordinate (0.59, 0.37) has been observed to be in the orange-red (598 nm) region for $Y_{0.77}Gd_{0.20}VO_4:0.03Sm^{3+}$ nanophosphor. These results perfectly established the suitability of these nanophosphors in improving the efficiency of silicon solar cells, light emitting diodes, semiconductor photophysics, and nanodevices.

1. Introduction

During last few decades, significant progress in solar energy harvesting by achieving substantial power conversion efficiencies was made possible by developing newer materials and adapting novel photovoltaic (PV) device architectures (Hisatomi et al., 2014; Chen et al., 2012a, 2012b; Pinel et al., 2011; Braga et al., 2008; Zou et al., 2001). However, the spectral mismatch between the energy distribution of photons in

* Corresponding author. Fax: +91 11 4560 9310.
E-mail address: haranath@nplindia.org (D. Haranath).
Peer review under responsibility of King Saud University.

ELSEVIER Production and hosting by Elsevier

http://dx.doi.org/10.1016/j.arabjc.2017.05.020
1878-5352 © 2017 The Authors. Production and hosting by Elsevier B.V. on behalf of King Saud University.
This is an open access article under the CC BY-NC-ND license (http://creativecommons.org/licenses/by-nc-nd/4.0/).

the incident solar spectrum and the band gap of semiconductor materials is found to be responsible for limiting the PV cell efficiencies much below the theoretical limit. Phosphors are those materials that are capable of converting ultra-violet radiations into photons of specific wavelengths, which in turn resolve the spectral mismatch issue of the PV cells. With an aim to achieve optimal spectral conversion in PV cells, many research groups all over the world have been exploring various nanophosphors based on oxides, oxysulfides, vanadates etc. (Heng et al., 2016; Zhydachevskii et al., 2014; Wegh et al. 1999; Wei et al., 2011; Bhargava et al., 2008). Among those rare-earth vanadates, i.e., $LnVO_4$, where Ln may be Y, Gd or La have received much attention as hosts for rare-earth doping because the major excitation mechanism is considerably different from other hosts leading to large Stokes shift and narrow emission lines (Zhu et al., 2016). A large number of recent papers on $GdVO_4$ and YVO_4 have appeared in the literature due to their adoption of PV technology, color television, and high-pressure mercury vapor lamp applications. However, there exist very few research papers on the composite (Y, Gd)VO_4 based nanophosphors (Bishnoi et al., 2017; Khan et al., 2008). (Y, Gd)VO_4 is an interesting luminescence host with a stable crystal structure and high thermal stability (Bishnoi et al., 2017). In the current paper, we report the active role of Gd^{3+} ions as mediators in drastically improving the rare-earth luminescence as well as energy transfer mechanism due to the presence of various concentrations of Gd^{3+} ions. It is well-known that an incorporation of dopant creates a perturbation in any known crystal host lattice. In the current study, Sm^{3+} was chosen as a representative rare-earth ion for doping because of its unique luminescence properties similar to that of Eu^{3+} ions and makes it an ideal probe for determining the local structure of the host crystal (Ropp, 1968). In this paper, we report the enhanced luminescence properties of Sm^{3+} doped (Y, Gd)VO_4 nanophosphor and efficient energy transfer occurring from VO_4^{3-} to Sm^{3+} via Gd^{3+} ions by applying Dexter-Reisfeld's theory and Inokuti-Hirayama model (Inokuti and Hirayama, 1965). Also, we established that these nanophosphors are an excellent candidate for achieving spectral conversion in silicon solar cells, and true color rendition in solid-state lighting devices.

2. Materials and methods

2.1. Starting materials

The rare-earth and transition metal oxides namely Gd_2O_3, Sm_2O_3 and Y_2O_3 having purity 99.99% each were taken as precursor materials for making their respective nitrate compounds by dissolving in stoichiometric volumes of 98% pure concentrated HNO_3. However, cetyltrimethylammonium bromide (CTAB) and ammonium metavanadate (NH_4VO_3) employed in the reaction have an individual purity of 99%.

2.2. Experimental approach

Sm^{3+} doped (Y, Gd)VO_4 nanophosphor samples have been prepared using a simple, versatile and controlled co-precipitation technique. In a typical sample synthesis, the stoichiometric amounts of nitrate salts of yttrium, gadolinium, and samarium were dissolved in demineralized water under continuously stirring for 1 h at room temperature (~25 °C). The Gd^{3+} and Sm^{3+} ion concentrations were varied from 5 to 50 mol% and 1 to 5 mol%, respectively for achieving optimal photoluminescence emission under UV (311 nm) excitation. An aqueous solution of CTAB has been used as a capping agent to control the size of the nanophosphor particles. NH_4VO_3 solution was added dropwise to the above solution that resulted in polymeric linear chain-like structures of VO_4^{3-} units. A mixture of ammonium hydroxide (NH_4OH) and hydrogen peroxide (H_2O_2) in the volume ratio 3:1 has been used to precipitate out the Sm^{3+} doped (Y, Gd)VO_4 nanophosphors. The resultant pale yellow color precipitate obtained was vacuum filtered and washed several times with demineralized water followed by ethanol to remove surface bound traces of unreacted impurities. The collected precipitate was then dried in air at 100 °C for 5 h followed by annealing at 800 °C for 2 h.

2.3. Characterization tools

The phase analysis of the nanophosphors has been checked with X-ray diffraction technique on powder samples using Rigaku (model: miniflex) X-ray diffractometer with Cu Kα radiations (λ = 1.5406 Å) with 2Θ ranging between 20 and 80°. Field-emission scanning electron microscope (model: Zeiss, Supra 40VP) has been used to study the morphology of the nanophosphor samples and element analysis by energy dispersive X-ray spectroscopy (EDXS, model: Oxford INCA 250). High-resolution transmission electron microscopy (HRTEM, model: Tecnai G2 F30 STWIN, field emission gun operated at 300 kV) was performed to study the internal structure and atomic scale configuration of lattice structure in real and reciprocal space. Room-temperature photoluminescence (PL) studies of the nanophosphors have been investigated using Edinburgh luminescence spectrometer (model: F900) equipped with xenon source as the source of excitation. The time-resoled PL measurements have been performed with the same instrument but with microsecond xenon flash lamp.

3. Result and discussion

3.1. Crystal structure and phase analysis

In general, it is understood that doping causes distortion in the crystalline host lattice. In other words, shape, size, and phase of host lattice will be modified by the extent of doping by rare-earth ions. The distortion occurs primarily due to the inner electric charge transfer between doped ions and cations of the crystal lattice (Wang et al., 2013). Therefore, X-ray diffraction (XRD) analysis was performed on as-synthesized $Y_{0.77}Gd_{0.20}VO_4$:0.03Sm^{3+} nanophosphor samples to characterize the phase purity of the samples. It is interesting to note that all the diffraction peaks matched very well with the standard JCPDS card. Fig. 1(a) shows the XRD patterns of the as-synthesized nanophosphor at 100 °C compared with the standard JCPDS card no. 85-2318 (Kumari and Manam, 2015). Inset of Fig. 1(a) shows the schematic of the structure of (Y, Gd)VO_4 host lattice. The crystallite size was calculated using the Scherrer equation (Evangeline et al., 2016)

$$Dp = \frac{k\lambda}{\beta \cos\theta}$$

where k is the constant (0.89), λ is the wavelength of the X-ray (0.154 nm or 1.54 Å), β is the full-width at half maxima (FWHM), and θ is the Bragg's angle of the respective XRD peak. The average crystallite size calculated from above equation was found to be ~28 nm. Fig. 1(b) shows the XRD patterns of samples annealed at 800 °C with varying concentrations of Gd^{3+} ions in the range 5–50 mol%. It is also

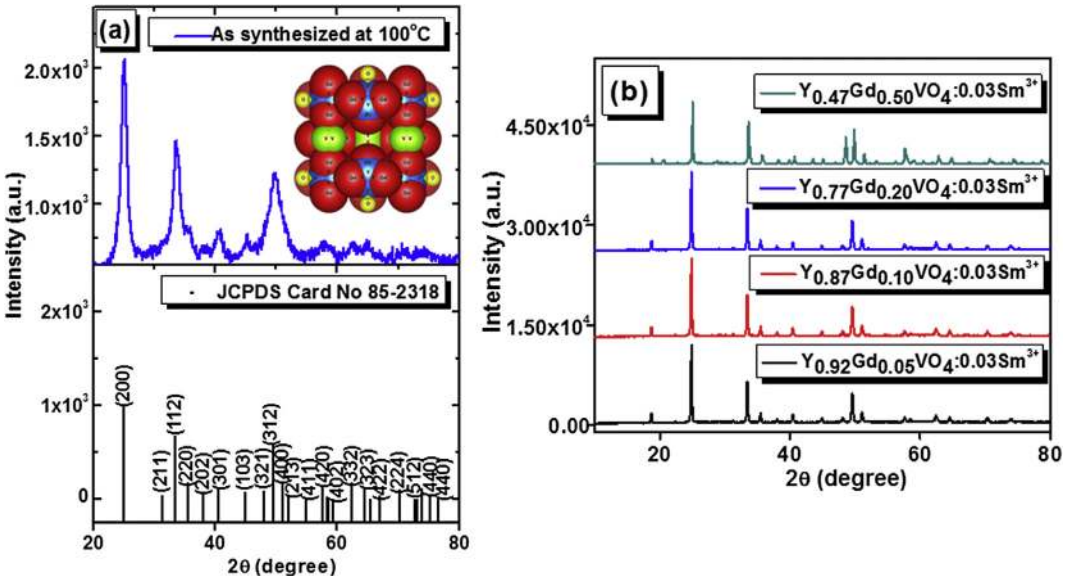

Figure 1 (a): XRD patterns of $Y_{0.77}Gd_{0.20}VO_4$:0.03Sm^{3+} nanophosphor as-synthesized at 100 °C sample and the corresponding JCPDS card no. 85-2318. The inset shows the schematic structure of the nanophosphor, and (b) XRD patterns of samples annealed at 800 °C with varying concentrations of Gd^{3+} ions in the nanophosphor.

clear from the figure that annealing at 800 °C resulted in better crystallization as compared to the as-synthesized nanophosphor samples. The XRD patterns exhibited all the major peaks indicating the formation of a single phase. It is also observed from XRD patterns that the nanophosphor has a tetragonal structure with a space group of *I41/amd*. The crystallographic and atomic parameters of the unit cell are summarized in Table 1.

3.2. Morphology and elemental analysis

The morphology of $Y_{0.77}Gd_{0.20}VO_4$:0.03Sm^{3+} nanophosphor annealed at 800 °C was investigated using field-emission scanning electron microscopy (FE-SEM) and high-resolution transmission electron microscopy (HR-TEM) techniques. The quantitative analysis of $Y_{0.77}Gd_{0.20}VO_4$:0.03Sm^{3+} nanophosphor has been investigated by energy dispersive X-ray analysis (EDAX) technique. FESEM image shown in Fig. 2(a) reveals the homogeneous distribution of the particles with an oval shape. EDAX spectrum shown in Fig. 2(b) clearly manifests the presence of O, V, Y, Sm and Gd elements in the sample along with their elemental composition (Evangeline et al., 2016). Fig. 2(c) and (d) represents TEM and HR-TEM of the nanophosphor, respectively.

3.3. Particle size distribution

In another innovative work, we tried to estimate the area covered by the nanophosphor particles with respect to their particle sizes. The study has been performed on a representative

Table 1 Crystallographic data and atomic parameters of $Y_{0.77}Gd_{0.20}VO_4$:0.03Sm^{3+} nanophosphor have been calculated.

Crystallographic data					
Crystal system					Tetragonal
Space Group					*I41/amd*
V (Å^3)					322.16
R-Factors (%)					
χ^2					3.45
R_p					12.22
R_{wp}					7.42
Atomic parameters					
Atom	OCC	*x*	*y*	*z*	Lattice parameters
O 4	0.987	0.0000	0.93874	1.46379	a = 7.1624 Å
V 1	0.341	0.0000	0.96521	0.5363	b = 7.1624 Å
Gd 1	0.030	0.0000	0.68983	0.42824	c = 6.3148 Å
Y 1	0.155	0.0000	0.0501	−0.04051	Alpha (α) = 90°
Sm 1	0.021	0.0000	0.453727	0.02134	Beta (β) = 90°
					Gamma (γ) = 90°

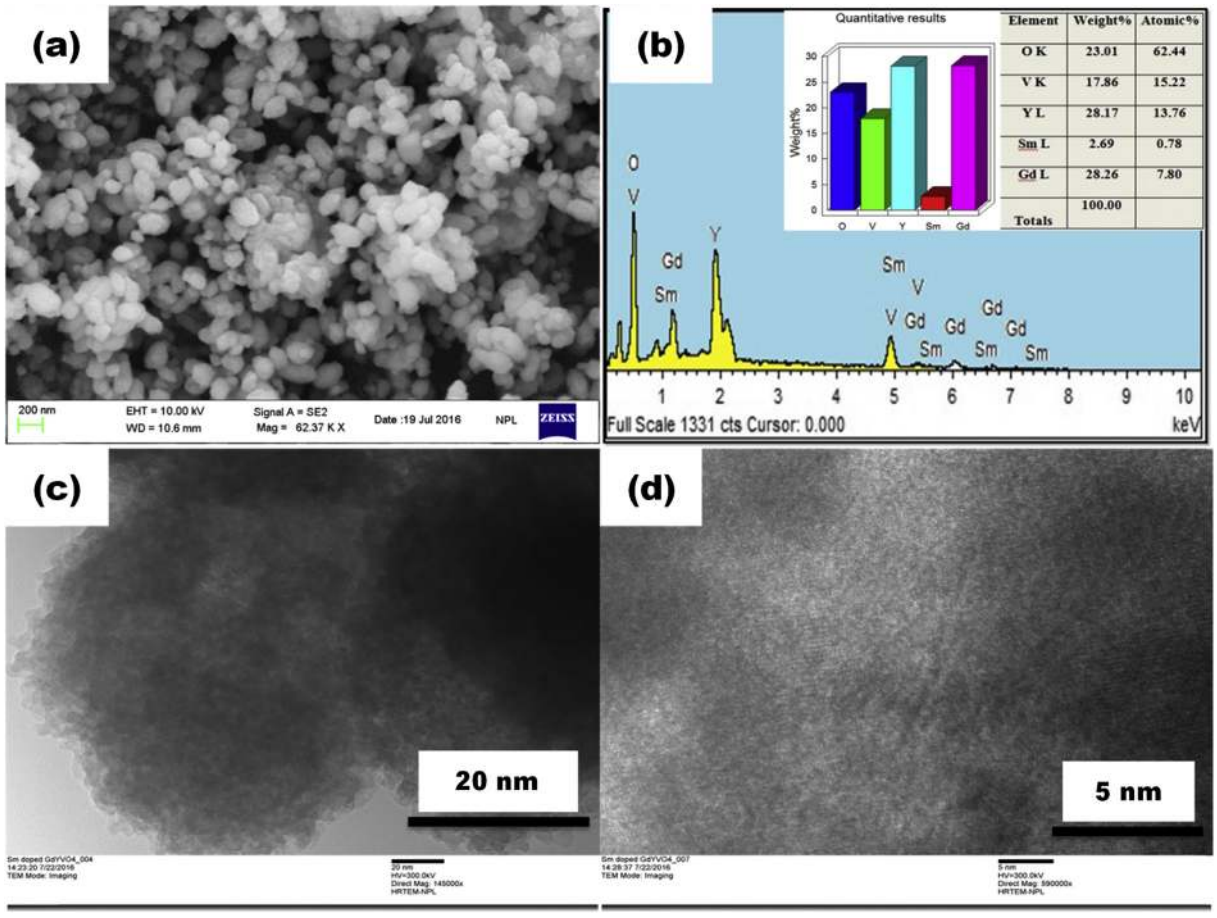

Figure 2 (a) SEM micrograph depicts the shape of $Y_{0.77}Gd_{0.20}VO_4$:0.03Sm^{3+} nanophosphor annealed at 800 °C, (b) EDAX represents the elemental composition of $Y_{0.77}Gd_{0.20}VO_4$:0.03Sm^{3+} nanophosphor, and (c-d) represents TEM and HR-TEM of the nanophosphor, respectively.

SEM micrograph of $Y_{0.77}Gd_{0.20}VO_4$:0.03Sm^{3+} nanophosphor sample using an image processing and analysis software in Java called *ImageJ* (Ver. 1.46) developed by National Institute of Health, USA. Fig. 3 shows the area covered by the nanophosphor particles having sizes in the range 5–85 nm. Most of the particles were found to be around 83 nm while some considerable number of particles having sizes 5, 18, 65 and 70 nm were also present. Inset of Fig. 3 shows the representative SEM micrograph chosen for this study and the black and white color patches represent the covered particle area and porosity of the nanophosphors, respectively. The result clearly shows that the particles have covered the surface about 39% with an open porosity of 61% in the representative SEM micrograph.

3.4. Photon cascade emission of Sm^{3+} in $Y_{0.77}Gd_{0.20}VO_4$:0.03Sm^{3+} nanophosphor

The excitation spectrum of $Y_{0.77}Gd_{0.20}VO_4$:0.03Sm^{3+} nanophosphor is represented in the inset of Fig. 4a. The spectrum gives rise to single excitation band peak located at 311 nm corresponding to the transition from the ground state $^1A_1$ to excited state $^1T_2$ of the VO_4^{3-} unit. Under the most intense n-UV excitation of ~311 nm corresponding to $^1A_1 \rightarrow {}^1T_2$ (t1 → 2e) transition, the emission spectrum

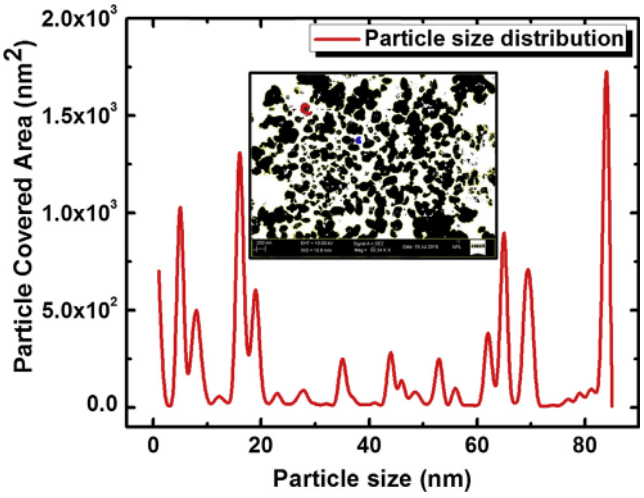

Figure 3 Area covered by particles versus particle sizes in a representative SEM micrograph of $Y_{0.77}Gd_{0.20}VO_4$:0.03Sm^{3+} nanophosphor sample.

recorded showed an efficient energy transfer from VO_4^{3-} network to Sm^{3+} ions mediated by Gd^{3+} ions. The emission peaks were observed at 563, 598 and 644 nm attributed to

$^4G_{5/2} \rightarrow {}^6H_{5/2}$, $^4G_{5/2} \rightarrow {}^6H_{7/2}$ and $^4G_{5/2} \rightarrow {}^6H_{9/2}$ transitions, respectively. The $^4G_{5/2} \rightarrow {}^6H_{5/2}$ transition arises due to the magnetic dipole (MD) transition and follows the first condition ($\Delta J = 0$), whereas the $^4G_{5/2} \rightarrow {}^6H_{9/2}$ is attributed to forced electric dipole (ED) transition. The $^4G_{5/2} \rightarrow {}^6H_{7/2}$ transition came in play due to both MD and forced ED transition. The emission corresponding to $^4G_{5/2} \rightarrow {}^6H_{7/2}$ transition has the maximum intensity (598 nm) as it satisfies the selection rule $\Delta J = \pm 1$ (allowed transition). The intensity ratio of ED to MD transition is used to measure the symmetry of the local environment of trivalent *O* ions. Greater the value of forced ED transition more is the asymmetric nature. In the present case, the value of MD transition is dominant that suggests more symmetric nature (Viswakarma et al., 2016; Suhasini et al., 2009).

3.5. Energy transfer mechanism from VO_4^{3-} to Sm^{3+} via Gd^{3+} ions in $Y_{0.77}Gd_{0.20}VO_4$:0.03Sm^{3+} nanophosphor

The energy transfer between two rare-earth ions can take place based on Dieke's energy level diagram. The energy transfer takes place from the rare-earth (RE) ion with the higher fluorescent excited state to another RE ion having the lower excited state. In the current case of $Y_{0.77}Gd_{0.20}VO_4$:0.03Sm^{3+} nanophosphor, VO_4^{3-} has the higher fluorescent excited state in comparison with the RE ions present in the nanophosphor. The sample excited under UV (~311 nm) light and then VO_4^{3-} unit attributed the allowed transition $^1A_1 \rightarrow {}^1T_2$, after that two possibilities may arise viz. either the VO_4^{3-} unit transfers its higher fluorescent energy to the dopant, Sm^{3+} ion or it relaxes to the ground state with the PL emission of blue light. It is interesting to note that due to maximum radiative energy loss, the VO_4^{3-} significantly influences the Gd^{3+} ions to take part in charge transfer band (CTB) processes. By monitoring PL emissions at 563, 598 and 644 nm, the excitation spectra of $Y_{0.77}Gd_{0.20}VO_4$:0.03Sm^{3+} nanophosphor were recorded and represented in Fig. 4b. It has been observed that energy transfer from VO_4^{3-} unit is effectively sensitizing the ^6P_J states of

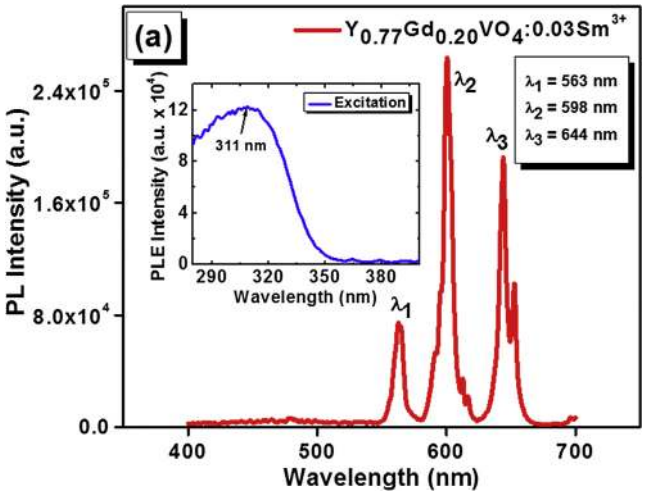

Figure 4a PL emission spectrum of $Y_{0.77}Gd_{0.20}VO_4$:0.03Sm^{3+} nanophosphor recorded in the range of 400–700 nm under 311 nm excitation. The corresponding excitation spectrum is shown as an inset in the figure.

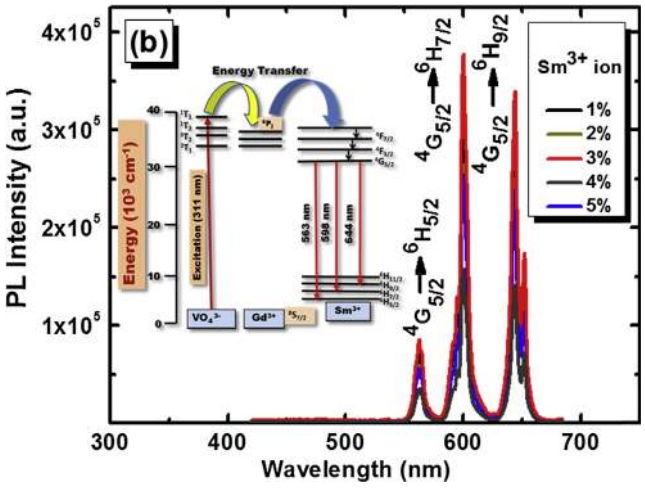

Figure 4b PL emission spectra of $Gd_{0.20}Y_{0.80-x}VO_4 : xSm$ (x = 1–5%) sample annealed at 800 °C and the inset energy diagram showing energy transfer mechanism in $Gd_{0.20}Y_{0.80-x}VO_4 : xSm$ nanophosphor.

Gd^{3+} ions because of the partial overlapping between the VO_4^{3-} emission and $^8S_{7/2}$-^6P_J absorption of Gd^{3+} ions resulting in an efficient orange-red PL emission. Moreover, in $Y_{0.77}Gd_{0.20}VO_4$ host lattice, the blue PL emission corresponding to VO_4^{3-} ion transition (figure not shown) is significantly reduced when Gd^{3+} ions are introduced into the lattice, because all the excitation energy absorbed by the VO_4^{3-} ions is further transferred to Gd^{3+} ions, lowering the intensity corresponding to blue emission. But when Sm^{3+} ions are added as a dopant in the lattice, the Gd^{3+} ions further transfer the excitation energy to the Sm^{3+} ions resulting in an enhanced orange-red emission. The study further established the role of Gd^{3+} ions as mediators in the energy transfer phenomenon between the VO_4^{3-} ions and Sm^{3+} ions. Based on the excitation spectra for $Y_{0.77}Gd_{0.20}VO_4$:0.03Sm^{3+} nanophosphor, 311 nm was considered as the appropriate excitation line for the series of Sm^{3+} concentration (x) varied from 1 to 5 mol % and Gd^{3+} concentration was fixed at 20 mol%. The intensity of Sm^{3+} bands increases with an increase in Sm^{3+} concentration up to 3 mol% (optimized concentration of Sm^{3+}) and decreases after that due to the concentration quenching phenomenon. The concentration quenching phenomenon is due to the self-absorption of emitted radiation from one Sm^{3+} ion by the nearest another Sm^{3+} ion, which in turn decreases the probability of radiative transition.

The energy transfer from the mediator (Gd^{3+}) to a dopant (Sm^{3+}) may take place via multipolar or exchange interactions. Based on Dexter's energy transfer formula (Li et al., 2011) for multipolar interaction and Reisfeld's approximation, a relation can be as written as follows:

$$C^{n/3} \propto \frac{\eta_o}{\eta}$$

where η_o and η are the luminescence quantum efficiencies of the Gd^{3+} in the absence and the presence of Sm^{3+}, C represents the sum of the mole% of the Gd^{3+} and the Sm^{3+}, and n equals to 6, 8 and 10 corresponding to dipole-dipole, dipole-quadrupole, and quadrupole-quadrupole interactions,

respectively. The $\frac{\eta_o}{\eta}$ value can be approximately calculated by the ratio of relative luminescence intensities as follows:

$$C^{n/3} \propto \frac{Is0}{Is}$$

where $Is0$ is the intrinsic emission intensity of Gd^{3+} and Is is the emission intensity of Gd^{3+} in the presence of Sm^{3+}.

3.6. Time-resolved photoluminescence decay study and colorimetry calculations

In this paper, the phenomenal role of Gd^{3+} ions in energy transfer mechanism has been studied with respect to the Gd^{3+} ion concentration using time-resolved photoluminescence (TRPL) decay measurements. TRPL is an important measurement to investigate the photon counts with respect to a lifetime of excitons. In this study, the Gd^{3+} ion concentration (x) has been varied from 5 to 50 mol% in $Y_{0.97-x}Gd_x$-VO_4:$0.03Sm^{3+}$ nanophosphors and the TRPL has been recorded at 311 nm excitation and 598 nm emission as shown in Fig. 5. It is clear from the figure that as the Gd^{3+} ion concentration increases up to 20 mol%, the decay time increases indicating that the Gd^{3+} ions are actively facilitating the energy transfer process to Sm^{3+} ions. However, it is also observed that beyond 20 mol%, the activity decelerated due to concentration quenching of the nearby Gd^{3+} ions. Hence, an amount of $x = 20$ mol% for Gd^{3+} ions was considered to be optimum for better energy transfer process in the $Y_{0.97-x}Gd_xVO_4$:$0.03Sm^{3+}$ nanophosphors.

Further, the decay profiles were recorded for $Y_{0.77}Gd_{0.20}$-VO_4:$0.03Sm^{3+}$ nanophosphor by monitoring the PL emissions at 598, 644 and 563 nm corresponding to $^4G_{5/2} \rightarrow {}^6H_{7/2}$, $^4G_{5/2} \rightarrow {}^6H_{9/2}$ and $^4G_{5/2} \rightarrow {}^6H_{5/2}$ transitions under 311 nm excitation and are shown in Fig. 6. The decay curves were fitted with different exponential equations. The best fit was obtained for double-exponential equation (Shen et al., 2005), which is given here under.

$$I(t) = I_0 + A_1 \exp(-t/\tau_1) + A_2 \exp(-t/\tau_2)$$

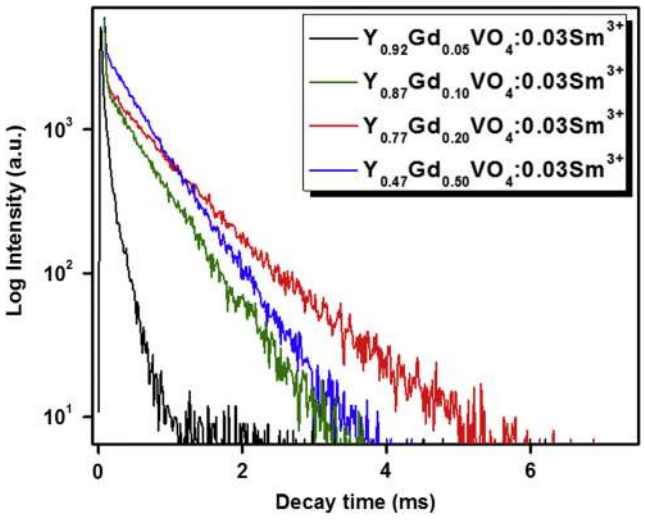

Figure 5 Time-resolved photoluminescence decay profiles of $Y_{0.97-x}Gd_xVO$:$0.03Sm^{3+}$ (x = 5–50 mol%) nanophosphors recorded at 311 nm excitation and 598 nm emission.

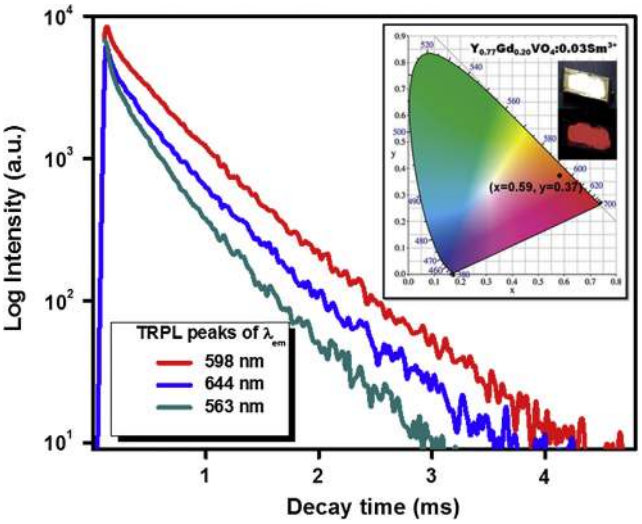

Figure. 6 Time-resolved photoluminescence decay studies of $Y_{0.77}Gd_{0.20}VO_4$:$0.03Sm^{3+}$ nanophosphor sample for the emission peaks at 598, 644 and 563 nm. The inset shows the CIE chromaticity diagram and the sample photographs under room light and UV (311 nm) excitation.

Table 2 Decay parameters of $Y_{0.77}Gd_{0.20}VO_4$:$0.03Sm^{3+}$ nanophosphor samples generated from the double-exponential function expression.

λ_{em} of $Y_{0.77}Gd_{0.20}VO_4$:$0.03Sm^{3+}$	τ_1 (m s)	τ_2 (m s)
563 nm	0.025	0.421
598 nm	0.025	0.529
644 nm	0.025	0.472

where I and I_0 represent the luminescence intensities at time t and 0, τ_1 and τ_2 are the fast and slow components of the luminescent lifetimes, and A_1 and A_2 are the fitting parameters, respectively. Due to the addition of Gd^{3+} ions, an extra pathway is created in the energy transfer, thereby enhancing the decay time. In the first instant, the absorbed energy is transferred from VO_4^{3-} to Gd^{3+} and there after this energy is transferred to the dopant Sm^{3+} ions, which increase overall decay times. The value of lifetime for double-exponential decay has been calculated using Inokuti-Hirayama model (Inokuti and Hirayama, 1965) and is given by the formula:

$$\tau = (A_1\tau_1^2 + A_2\tau_2^2)/(A_1\tau_1 + A_2\tau_2)$$

The lifetimes thus calculated are presented in Table 2. The average value of a lifetime of VO_4^{3-}decreases with an increase in the Sm^{3+} concentration via optimized concentration of Gd^{3+} ions, which is strong evidence of energy transfer from VO_4^{3-} to Sm^{3+} via Gd^{3+} ions.

The CIE (Commission Internationale de I'Eclairage 1931 chromaticity) color coordinate positions were calculated by a spectrophotometric method using spectral energy distribution of $Y_{0.77}Gd_{0.20}VO_4$:$0.03Sm^{3+}$ nanophosphor sample based on emission spectra presented in Fig. 6. The CIE chromaticity coordinates were determined using normalized PL data recorded at an interval of 1 nm by feeding it into an

indigenously developed program based on the Equidistant Wavelength Method (Kelmer, 1969). The color co-ordinates values (x,y) corresponding to $Y_{0.77}Gd_{0.20}VO_4{:}0.03Sm^{3+}$ nanophosphor were calculated to be (0.59, 0.37) suggesting the orange-red region of the chromaticity diagram.

4. Conclusions

In the present study, luminescence properties of orthovanadates of the type, $Y_{1-x-y}Gd_xVO_4{:}ySm^{3+}$ (where $x = 0.05–0.50$, $y = 0.01–0.05$), and the energy transfer mechanism from VO_4^{3-} to Sm^{3+} via Gd^{3+} ions were investigated in detail. X-ray diffraction analysis confirmed the crystalline phase for synthesized nanophosphor in a tetragonal structure with *I41/amd* space group. The morphological studies revealed controlled particle sizes with truncated oval shapes, and the elemental analysis showed the presence of all elements of the sample. The role of Gd^{3+} ions as mediators in significantly improving the PL emission has been established with PLE, PL and TRPL decay measurements. The combination of unique features of high surface area-to-volume ratios, low polydispersity index, slight magnetic effect, perfect crystalline structure and optimum photoluminescence suggests that these nanophosphors could find interesting applications in the fields of silicon solar cells, semiconductor photophysics, inorganic light-emitting diodes, and many electronic devices.

Acknowledgments

The authors sincerely acknowledge the Council of Scientific & Industrial Research (CSIR), and Board of Research in Nuclear Sciences (BRNS), Government of India for the fellowship grant Nos. 31/1(445)/2015-EMR-1, 31/1(413)/2015-EMR-1 and 34/14/16/2016-BRNS/34041 for the financial support rendered to execute this work.

References

Braga, A.F.B., Morrira, S.P., Zampieri, P.R., Bacchin, J.M.G., Mei, P. R., 2008. Sol. Energy Mater. Sol. Cells 92, 418–424.
Bhargava, R.N., Haranath, D., Mehta, A., 2008. J. Kor. Phys. Soc. 53, 2847–2851.
Bishnoi, S., Swati, G., Singh, P., Jaiswal, V.V., Sahu, M., Gupta, V., Vijayan, N., Haranath, D., 2017. http://dx.doi.org/10.1107/S1600576717004277.
Chen, H.M., Chen, C.K., Liu, R.S., Zhang, L., Zhang, J., Wilkinson, D.P., 2012a. Chem. Soc. Rev. 41, 5654–5671.
Chen, X., Li, C., Gratzel, M., Kostecki, R., Mao, S.S., 2012b. Chem. Soc. Rev. 41, 7909–7937.
Evangeline, B., Azeem, P., Abdul, R., Rao, P., Swati, G., Haranath, D., 2016. J. Alloys Compd. 16, 33584–33588.
Heng, C.L., Wang, T., Su, W.Y., Wu, H.C., Yin, P.G., Finstad, T.G., 2016. J. Appl. Phys. 119, 123105–123107.
Hisatomi, T., Kubota, J., Domen, K., 2014. Chem. Soc. Rev. 43, 7520–7535.
Inokuti, M., Hirayama, F., 1965. J. Chem. Phys. 43, 1978–1989.
Kelmer, J., 1969. Luminescent Screens: Photometry and Colorimetry. Iliffe, London, p. 118.
Khan, K.F., Haranath, D., Yadav, R., Singh, S., Chawala, S., Dutta, V., 2008. Appl. Phys. Lett. 93, 073103–073105.
Kumari, P., Manam, J., 2015. RSC Adv. 5, 107575–107584.
Li, G., Geng, D., Shang, M., Peng, C., Cheng, Z., Lin, J., 2011. Mater. Chem. 21, 13334–13344.
Pinel, P., Cruickshank, C.A., Beausoleil-Morrison, I., Wills, A., 2011. Renewable Sustainable Energy Rev. 15, 3341–3359.
Ropp, R.C., 1968. J. Electrochem. Soc. Solid State Sci. 115, 940–945.
Shen, W.Y., Pang, M.L., Lin, J., Fang, J., 2005. J. Electrochem. Soc. 152, H25–H28.
Suhasini, T., Kumar, S.J., Sasikala, T., Jang, K., Lee, H.S., Jayasimahadri, M., Jeong, J.H., Yi, S.S., Moorthy, R., 2009. Opt. Mater. 31, 1167–1172.
Vishwakarma, A.K., Jayasimahdri, M., 2016. J. Lumin. 176, 112–117.
Wang, X., Bu, Y., Xiao, Y., Kan, C., Lub, D., Yan, X., 2013. J. Mater. Chem. C 1, 3158–3166.
Wegh, R.T., Donker, H., Oskam, K.D., Meijerink, A., 1999. J. Lumin. 82, 93–104.
Wei, X., Liu, Y., Jiang, G., Chen, Y., Yin, M., Xu, W., 2011. J Nanosci. Nanotechnol. 11, 9556–9561.
Zhu, X., Su, Q., Feng, W., Li, F., 2016. Chem. Soc. Rev. 46, 1025–1039.
Zhydachevskii, Y., Lipińska, L., Baran, M., Berkowski, M., Suchocki, A., Reszka, A., 2014. Mat. Chem. Phys. 143, 622–628.
Zou, Z., Ye, J., Sayama, K., Arakawa, H., 2001. Nature 414, 625–627.